Measuring Glacier Elevation Change by Tracking Shadows on Satellite Monoscopic Optical Images

Niccolò Dematteis, Daniele Giordan, Bruno Crippa, and Oriol Monserrat

***Abstract*— Measuring glacier elevation change is crucial information for estimating glacier mass balance, calibrating mass balance and climate models, and assessing the impact of global warming. We examined the potentiality of clinometry to quantify glacier elevation changes. This technique allows calculating the elevation of the points that lie on the margins of the shadows cast by the local topography on monoscopic optical images. Mapping the shadow position across different images permits quantifying surface elevation changes. We applied clinometry to Sentinel-2 images of the Aletsch Glacier (Switzerland) and we measured a glacier thinning of -1.9 ± 1.7 ma^{-1} between 2017 and 2021, in agreement with previous observations.**

***Index Terms*— Aletsch glacier, digital elevation model (DEM), glacier elevation change, glacier mass balance, satellite optical images, shadow tracking.**

I. Introduction

DOCUMENTING glacier elevation evolution would help to understand their response to climate better and their contribution to sea-level rise [1], in particular, that of mountain glaciers, which is relevant despite their limited size [2], [3]. Measuring glacier elevation change is a common method for estimating glacier mass balance [4], [5], [6]. Due to the often remote location, satellite-based observations of glacier changes complement field-based surveys [7]. However, space-borne observations are challenging and often are sparsely distributed across the globe [8], [9]. This is particularly true for mountain glaciers, since cryosphere-dedicated spacecraft missions (e.g., ICESat, CryoSat) have been conceived to monitor ice caps especially [10]. On the other hand, satellite synthetic aperture radar interferometry (InSAR) and optical stereoscopy provide almost full ground coverage, but often suffer from inferior quality and outliers [11]. For example, the penetration of microwaves into snow/ice is highly variable (e.g., X-band penetration varies between 0.1 and 6 m in wet and dry snow, respectively [12]) and can introduce potential bias in InSAR-derived glacier elevation [13], [14]. Besides, voids in optical imagery can occur in shadow areas [13]. Furthermore, InSAR and optical stereoscopy require consolidated but often complex processing techniques [7]. Therefore, diverse techniques that complement such observations can support data validation and increase data spatial and temporal coverage.

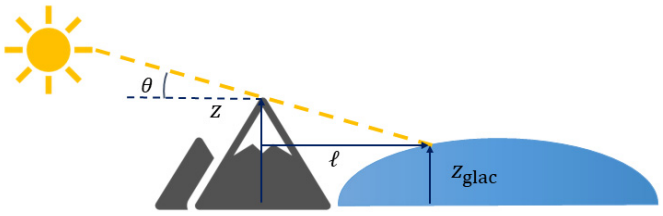

Fig. 1. Conceptual illustration of the shadow-height method.

A possible alternative approach is a shadow-height method (or clinometry) [15], which allows determining the glacier elevation at the margins of a shadowed surface by knowing the height of the shadowing object (see Fig. 1). This method was originally proposed by [16] to solve the inverse problem, i.e., determining the height of the object—a building in that case—that casts the shadow, and successively adopted in other similar studies [17], [18]. Applications of clinometry in earth science are less common [15], [19], [20], but recently, Altena et al. [21] and Giacaman [22] proposed to use such a method to assess glacier elevation change using manual shadow delineation in specific points.

The aim of this study is to develop a semiautomated shadow-height procedure to derive spatially dense glacier elevation change measurements, examining the limitations and potentialities of this technique using Sentinel-2 images. To this end, we analyzed the case of the Aletsch Glacier (Switzerland) and obtained its surface elevation changes between 2017 and 2021.

II. Dataset and Methods

The principle of the shadow-height method to measure the glacier surface elevation z is illustrated in Fig. 1 and formulated as follows:

$$z = z_{\text{topo}} - \ell \tan\theta \tag{1}$$

where z_{topo} is the known height of the local topography, ℓ is the planimetric shadow length along the light direction, and θ the sun altitude angle. Interpolating elevation point values

Manuscript received 4 February 2022; revised 26 May 2022, 24 August 2022, and 9 December 2022; accepted 20 December 2022. Date of publication 22 December 2022; date of current version 7 February 2023. *(Corresponding author: Daniele Giordan.)*

Niccolò Dematteis and Daniele Giordan are with the Research Institute for Geo-Hydrological Protection, Italian National Research Council, 10135 Turin, Italy (e-mail: niccolo.dematteis@irpi.cnr.it; daniele.giordan@irpi.cnr.it).

Bruno Crippa is with the Department of Earth Sciences, University of Milan, 20122 Milan, Italy (e-mail: bruno.crippa@unimi.it).

Oriol Monserrat is with the Geomatic Division, Centre Tecnològic de Telecomunicacions de Catalunya, 08860 Castelldefels, Spain (e-mail: oriol.monserrat@cttc.es).

Digital Object Identifier 10.1109/LGRS.2022.3231659

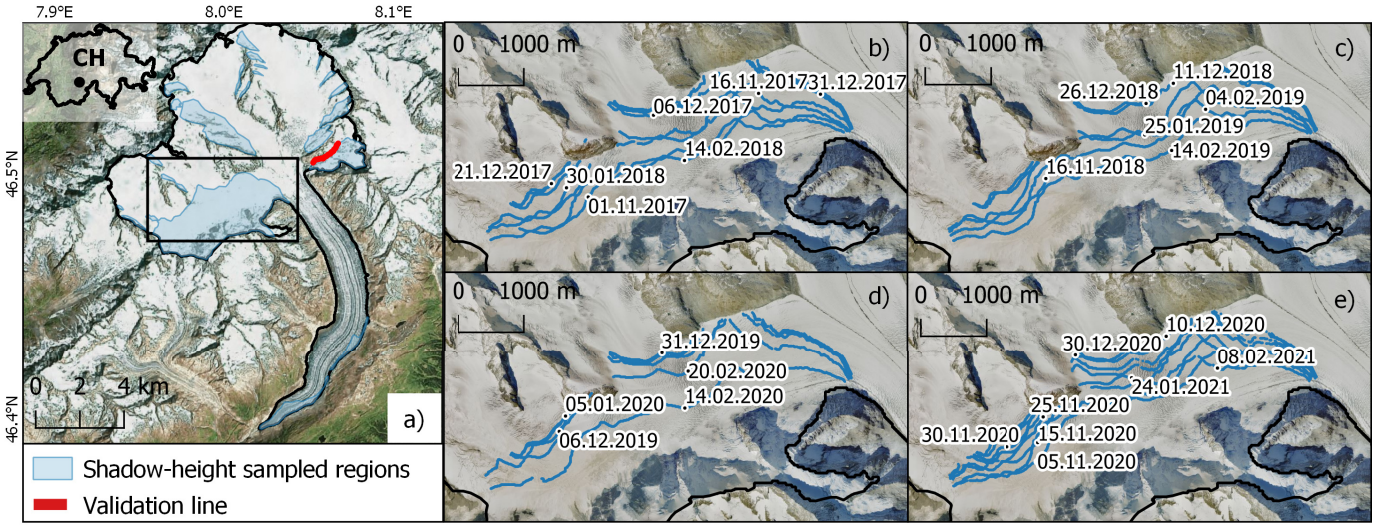

Fig. 2. (a) Aletsch Glacier (Switzerland) outlines (from the Randolph Glacier Inventory). Shaded blue areas indicate the regions where it is possible to apply the shadow-height method, while the black rectangle identifies the area displayed in (b)–(d) and Fig. 3(a). The red line indicates the shadow line used to validate the method off the glacier. (b)–(e) Delineations of the shadow margins in seasons 2017–2018, 2018–2019, 2019–2020, and 2020–2021, respectively. Each delineation is labeled with the acquisition date (date format dd.mm.yyyy). Background Bing aerial.

across an area of interest permits to obtain spatially distributed glacier surface elevation.

A. Implementation

To measure the glacier surface elevation change, we developed a semi-automatic procedure. We used a MATLAB built-in edge detection function with the Sobel operator to detect the shadow margins automatically, then we manually checked the results to correct outliers and remove self-shadowed areas. Subsequently, we determined the surface elevation in every point of the shadow margins with (1), adopting several images acquired in the same period. To assess the spatially-distributed elevation change, we conducted the following steps: 1) we applied the double differentiation method [8]; i.e., the differentiation of the elevation point measurements from a reference DEM (topographic normalization); 2) we interpolated the elevation differences with a quadratic polynomial function [13]; and 3) we calculated the difference of two interpolated surfaces to obtain the areal glacier elevation change.

B. Area of Study

The Aletsch Glacier [see Fig. 2(a)] is the largest glacier in the European Alps, which lies on the southern flanks of the Aletschhorn massif (Switzerland), ranging from 1900 to 3800 m a.s.l., approximately. It is a 20 km-long valley glacier that covers an area of $\sim$80 km^2, with a thickness of up to 850 m [23]. It represents 20% of the total ice volume of Switzerland and has a substantial relevance for the hydrological cycle of the Rhone River [24]. Since 1880, the glacier thickness has reduced by more than 50 m on average [23], while recent numerical models predict an average thinning rate until 2050 from -2.4 to -5.4 ma^{-1}, depending on the climate scenario [25]. We focused on the 8 km^2-wide westernmost accumulation tongue, the Grosser Aletschfirn, which extends between 2600 and 3200 m a.s.l., and is more than 600 m-thick [25], while its average slope is $\sim$7°.

C. Dataset

We used registered 10 m-resolution green band (B03) Sentinel-2 A and B images (absolute orbit 204, relative orbit 108, processing level L1C). Sentinel-2 metadata provide the solar azimuth and zenith angles for every 5 $\times$ 5 km portion of the image, which can be immediately used in (1). Alternatively, the sun position can be calculated independently by adopting precise values of geographical coordinates and time and date.

We used the images available in the winter seasons (i.e., from November to February) of 2017–2018, 2018–2019, 2019–2020, and 2020–2021. In every period, we had five to eight cloud-free images and the shadow traces were homogeneously distributed across the glacier tongue [see Fig. 2(b)]. Finally, we used a freely available 2 m-resolution digital elevation model (DEM) acquired in 2019 and provided by the Switzerland Federal Office of Topography (swisstopo) [26], with a vertical uncertainty above 2000 m a.s.l. of $\pm$1–3 m [27].

III. Results

The results of this study are illustrated in Fig. 3. Fig. 3(a) shows the mean annual glacier elevation change between 2017–2018 and 2020–2021, which varies between -2.6 and -0.9 ma^{-1}, depending on the height. We reported also the isohypses of the derived glacier surface elevation in 2017–2018 and 2020–2021. Their shapes are consistent, but the isohypses in 2020–2021 have moved upward, indicating a thinning of the glacier between the two periods.

Fig. 3(b) reports the mean annual glacier elevation change distributions with respect to the glacier absolute height, between 2017–2018 and 2019–2020 (mean variation of -2.2 ma^{-1}), 2017–2018 and 2020–2021 (mean variation of -1.9 ma^{-1}) and 2018–2019 and 2020–2021 (mean variation of -2.3 ma^{-1}). In every case, the elevation change was not homogeneous throughout the glacier tongue, but it was more pronounced at lower elevations. We only considered

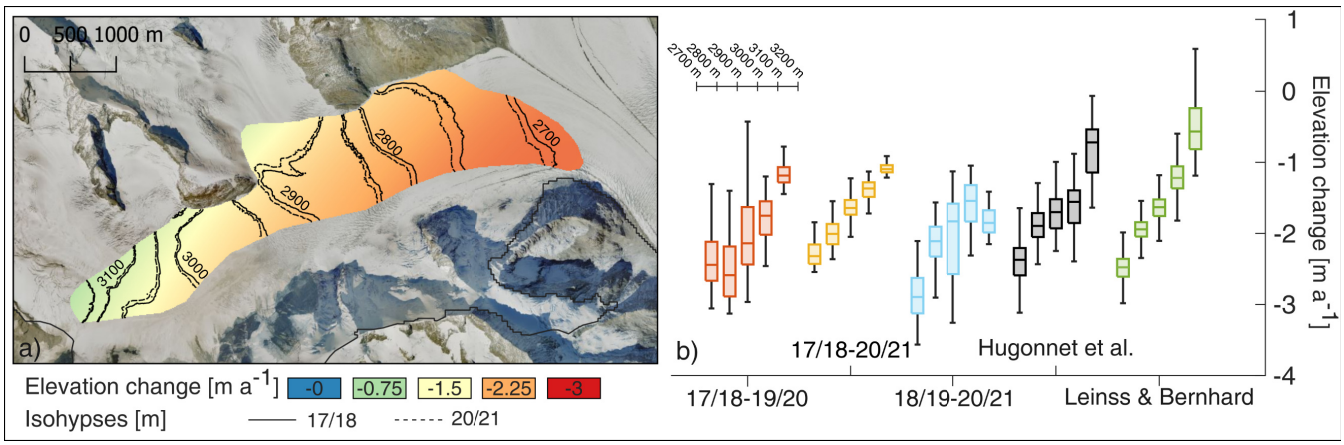

Fig. 3. (a) Mean annual glacier elevation change calculated between 2017–2018 and 2020–2021. Black lines represent the isohypses of the glacier surface elevation evaluated in 2017–2018 (solid lines) and 2020–2021 (dashed lines). Background Bing aerial. (b) Mean annual elevation change between 2017–2018 and 2019–2020 (red boxes), 2017–2018 and 2020–2021 (yellow boxes), 2018–2019 and 2020–2021 (blue boxes), and obtained by [28] between 2015 and 2019 (gray boxes) and [14] between 2011 and 2019 (green boxes). Each box indicates the elevation change in height bands of 100 m between 2700 and 3200 m a.s.l.

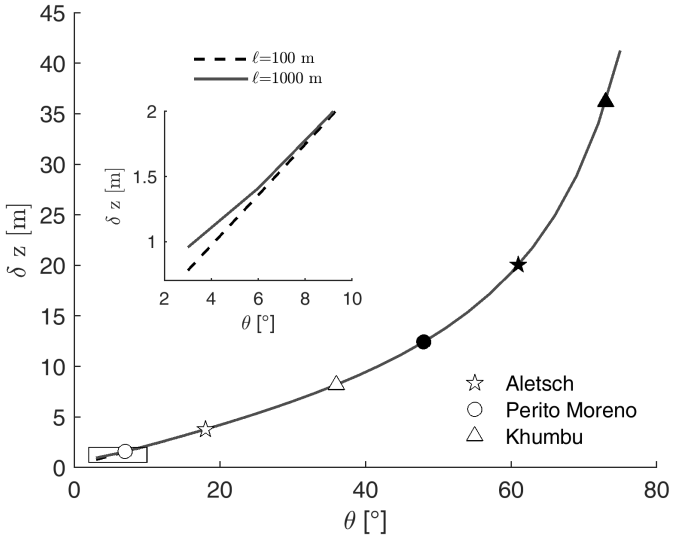

Fig. 4. Absolute clinometry precision at 2000 m a.s.l. Dashed and solid lines indicate the precision for different shadow lengths (100 and 1000 m), which depend on the uncertainty of the sun altitude angle. White and black markers refer to the sun altitude angle at winter and summer solstices, respectively, for the Aletsch (46.5°N–8°E, European Alps), Perito Moreno (50.5°S–73°W Southern Patagonian Icefield), and Khumbu (28°N–87°E, Himalaya) glaciers. The inset reports the detail in the altitude angle range of 2°–10°.

elevation changes during a time span ≥2 years to reduce the potential error due to surface modifications (e.g., due to snow accumulation and avalanches).

A. Comparison With Previous Studies

Hugonnet et al. [28] published a 100 m-resolution raster of elevation change of the Aletsch Glacier between 2015 and 2019, obtained with various stereo and radar satellite images; in the study area [see Fig. 3(a)], they obtained an average thinning of -2.0 ± 2.5 ma^{-1}, which varied between -2.4 ma^{-1} at 2750 m a.s.l. and -0.7 ma^{-1} at 3150 m a.s.l. [see Fig. 3(b)]. Leinss and Hajnsek [29] observed an average thinning of the whole glacier of -3.3 ma^{-1} between 2011 and 2016 by analyzing more than 100 DEMs produced with TanDEM-X data. Leinss and Bernhard [14] too analyzed TanDEM-X images, between 2011 and 2019, and measured an elevation loss in the study area of -1.9 ma^{-1} [see Fig. 3(b)]. Furthermore, Kropáček et al. [5] used ICESat data and estimated nearly zero elevation changes at 3400 m a.s.l. and -2.2 ma^{-1} at 2800 m a.s.l. between 2003 and 2009.

B. Uncertainty Analysis

The proposed method to calculate the surface elevation change consists of three main steps: 1) point elevation measurement using (1); 2) spatial interpolation of point values; and 3) differentiation of surfaces obtained at different times. Accordingly, the uncertainty analysis can be conducted separately for each stage.

The error budget of the point elevation measurement is estimated by applying the error propagation to (1) and assuming the variables independent

$$\delta z = \sqrt{\delta z_{\text{topo}}^2 + (\ell \tan \delta\theta)^2 + (\delta \ell \tan \theta)^2} \tag{2}$$

where δz_{topo} is the DEM vertical precision (i.e., 1–3 m) and $\delta\theta$ is the altitude angle error, which depends on the apparent sun position due to atmospheric refraction. According to [22], at very high latitudes, the second error term can assume significant values (see Fig. 4). However, in the Aletsch Glacier, its value would be 0.175 m at a 1000 m distance, thus it can be considered negligible.

The third error element, $\delta\ell$, concerns the error of shadow line delineation. Several factors contribute to this term, according to

$$\delta \ell = \delta \ell_{\text{topo}} + \delta \ell_{\text{geo}} + \delta \ell_{\text{res}} + \delta \ell_{\text{pick}} \tag{3}$$

where δl_{topo} is the precision of planimetric positioning of the topography casting the shadow, which corresponds to half the DEM resolution (1 m). δl_{geo} concerns the error of orthorectification. This term can strongly impact, especially when adopting an old and/or coarse DEM to orthorectify.

However, images acquired at the same orbit are orthorectified by the same process and, therefore, the potential error should compensate. δl_{res} accounts for the integer sensitivity of the shadow length measurement, which corresponds to half the image resolution (5 m) and δl_{pick} concerns the picking (manual or automatic either) of the shadow line. This is caused by the diffuse nature of the shadow, since the angular span of the sunlight is non-zero (approximately 0.5°). According to [22], the shadow margin can span between less than 1 m to a few tens of meters, depending on the sun altitude angle and shadow length. Nevertheless, although this uncertainty can introduce bias in the absolute elevation, it compensates when two surfaces are differentiated, provided that a constant shadow edge detection method is adopted. Consequently, δl_{pick} can be conservatively assumed equal to 1 px (i.e., 10 m). In the end, substituting the uncertainty values in (2), δz is 5 m, considering a sun altitude angle of 20°.

Besides the theoretical uncertainty derivation, we compared the results of (1) along a shadow line lying outside the glacier [see Fig. 2(a)], with swisstopo as a reference datum, obtaining a deviation of -2.6 ± 5.5 m (median $\pm$ median absolute deviation, MAD).

To evaluate the uncertainty of the interpolation during the second stage, we analyzed the residuals between the point elevation data and the interpolated surface, obtaining -0.1 ± 4.3 m (median $\pm$ MAD), in line with the point elevation uncertainty.

Finally, in the last stage—i.e., the differentiation of two surfaces acquired at different times—systematic errors are compensated (i.e., δl_{geo} and δl_{pick}) and the resulting elevation change uncertainty is divided by the temporal lag between the surfaces' acquisitions.

IV. Discussion

According to the results of this study, the main clinometry advantages pertain to two aspects: 1) it is simple to calculate, especially compared to optical stereoscopy and InSAR, and 2) it provides high-resolution elevation change maps in regions that are typically difficult to be investigated with other methods; e.g., it works in shadowed areas (which affect optical stereoscopy); and it works in areas of enhanced/complex topography (which affects radar and Lidar) [13]. Therefore, it is particularly useful to fill the potential gaps in those regions and it can be used for cross-validation with other methods.

The interpolation process deserves some comments too. Since the images are acquired at different dates, potential surface modifications can occur, which can introduce biases in the surface height values. However, the shadow lines—adopted to interpolate—that are in similar positions have been acquired on similar dates. Consequently, the time gap between two interpolated surfaces remains approximately constant across the region. Therefore, the shadow-height method is more effective to measure elevation changes rather than absolute elevation values. In any event, it is advisable to consider elevation change during periods spanning for at least 2–3 years to reduce errors related to surface modifications [9]. By that means, the estimated uncertainty (5 m in this case) decreases further.

On the other hand, clinometry limitations pertain to the site geometry. It requires the presence of shadows cast by the neighbor topography; therefore, it is effective to survey narrow mountain glaciers with favorable orientation (e.g., east-west and northwards/southwards orientations in northern/southern hemispheres, respectively), while it is not suitable to monitor ice sheets, ice caps or vast glaciers. This issue can limit the spatial coverage of the sampled area. E.g., approximately 25% of the Aletsch Glacier area can be examined by the shadow-height method [see Fig. 2(a)]. Another limitation concerns the sensitivity of (2) to the sun altitude angle: at low latitudes and close to the summer solstice, when the sun altitude angle is high, the precision drops substantially and δz can reach a few tens of meters. On the contrary, in winter at high latitudes, the precision increases (see Fig. 4).

V. Conclusion

We have shown the potentialities of the shadow-height method (clinometry) in detecting glacier surface elevation change, using Sentinel-2 images of the Aletsch Glacier. The results well reflect past studies, with a thinning rate of -1.9 ± 1.7 ma^{-1}. Despite its limitations, this technique demonstrated a high benefit-cost ratio, because it requires monoscopic satellite optical images, which are freely available and offer high spatial resolution and coverage and short revisit times. Future research should be dedicated to investigating methods to achieve subpixel precision of shadow delineation (e.g., like in [22]), and to develop completely autonomous methods of shadow delineation.

Data Availability

The MATLAB code adopted to perform the processing of this study is available at https://github.com/niccolodematteis/Elevation-From-Shadow

References

[1] C. Nuth, G. Moholdt, J. Kohler, J. O. Hagen, and A. Kääb, "Svalbard glacier elevation changes and contribution to sea level rise," *J. Geophys. Res.*, vol. 115, no. F1, pp. 1–16, 2010.

[2] M. F. Meier et al., "Glaciers dominate eustatic sea-level rise in the 21st century," *Science*, vol. 317, no. 5841, pp. 1064–1067, 2007.

[3] M. Zemp et al., "Historically unprecedented global glacier decline in the early 21st century," *J. Glaciol.*, vol. 61, no. 228, pp. 745–762, 2015.

[4] E. Berthier, Y. Arnaud, R. Kumar, S. Ahmad, P. Wagnon, and P. Chevallier, "Remote sensing estimates of glacier mass balances in the Himachal Pradesh (Western Himalaya, India)," *Remote Sens. Environ.*, vol. 108, no. 3, pp. 327–338, Jun. 2007.

[5] J. Kropáček, N. Neckel, and A. Bauder, "Estimation of mass balance of the Grosser Aletschgletscher, Swiss Alps, from ICESat laser altimetry data and digital elevation models," *Remote Sens.*, vol. 6, no. 6, pp. 5614–5632, Jun. 2014.

[6] M. J. Willis, A. K. Melkonian, M. E. Pritchard, and J. M. Ramage, "Ice loss rates at the Northern Patagonian icefield derived using a decade of satellite remote sensing," *Remote Sens. Environ.*, vol. 117, pp. 184–198, Feb. 2012.

[7] F. Paul et al., "The glaciers climate change initiative: Methods for creating glacier area, elevation change and velocity products," *Remote Sens. Environ.*, vol. 162, pp. 408–426, Jun. 2015.

[8] A. Kääb, E. Berthier, C. Nuth, J. Gardelle, and Y. Arnaud, "Contrasting patterns of early twenty-first-century glacier mass change in the Himalayas," *Nature*, vol. 488, no. 7412, pp. 495–498, Aug. 2012.

[9] G. Moholdt, C. Nuth, J. O. Hagen, and J. Kohler, "Recent elevation changes of Svalbard glaciers derived from ICESat laser altimetry," *Remote Sens. Environ.*, vol. 114, no. 11, pp. 2756–2767, Nov. 2010.

[10] H. J. Zwally et al., "ICESat's laser measurements of polar ice, atmosphere, ocean, and land," *J. Geodyn.*, vol. 34, nos. 3–4, pp. 405–445, 2002.
[11] D. Wang and A. Kääb, "Modeling glacier elevation change from DEM time series," *Remote Sens.*, vol. 7, no. 8, pp. 10117–10142, Aug. 2015.
[12] A. Dehecq, R. Millan, E. Berthier, N. Gourmelen, E. Trouve, and V. Vionnet, "Elevation changes inferred from TanDEM-X data over the Mont-Blanc area: Impact of the X-band interferometric bias," *IEEE J. Sel. Topics Appl. Earth Observ. Remote Sens.*, vol. 9, no. 8, pp. 3870–3882, Aug. 2016.
[13] F. Paul et al., "Error sources and guidelines for quality assessment of glacier area, elevation change, and velocity products derived from satellite data in the Glaciers_cci project," *Remote Sens. Environ.*, vol. 203, pp. 256–275, Dec. 2017.
[14] S. Leinss and P. Bernhard, "TanDEM-X: Deriving InSAR height changes and velocity dynamics of great Aletsch glacier," *IEEE J. Sel. Topics Appl. Earth Observ. Remote Sens.*, vol. 14, pp. 4798–4815, 2021.
[15] T. Toutin, "Elevation modelling from satellite visible and infrared (VIR) data," *Int. J. Remote Sens.*, vol. 22, no. 6, pp. 1097–1125, Jan. 2001.
[16] A. Huertas and R. Nevatia, "Detecting buildings in aerial images," *Comput. Vis., Graph., Image Process.*, vol. 41, no. 2, pp. 131–152, Feb. 1988.
[17] V. K. Shettigara and G. M. Sumerling, "Height determination of extended objects using shadows in SPOT images," *Photogramm. Eng. Remote Sens.*, vol. 64, no. 1, pp. 35–44, 1998.
[18] J. Meng and M. Davenport, "Building assessment with subpixel accuracy using satellite imagery," *Proc. SPIE*, Vol. 2656, pp. 65–76, Mar. 1996.
[19] Z. Guan, X. Cheng, Y. Liu, T. Li, B. Zhang, and Z. Yu, "Effectively extracting iceberg freeboard using bi-temporal Landsat-8 panchromatic image shadows," *Remote Sens.*, vol. 13, no. 3, pp. 1–17, 2021.
[20] S. Pailot-Bonnétat, A. J. L. Harris, S. Calvari, M. De Michele, and L. Gurioli, "Plume height time-series retrieval using shadow in single spatial resolution satellite images," *Remote Sens.*, vol. 12, no. 23, pp. 1–23, 2020.
[21] B. Altena et al., "Topographic elevation change through tracking shadow cast from mountain ridges. Showcasing Red Glacier, Mt. Iliamna," in *Proc. EGU Gen. Assem. Conf. Abstr.*, 2021, p. 10774.
[22] C. A. R. Giacaman, "High-precision measurement of height differences from shadows in non-stereo imagery: New methodology and accuracy assessment," *Remote Sens.*, vol. 14, no. 7, p. 1702, Apr. 2022.
[23] A. Bauder, M. Funk, and M. Huss, "Ice-volume changes of selected glaciers in the Swiss Alps since the end of the 19th century," *Ann. Glaciol.*, vol. 46, pp. 145–149, Jan. 2007.
[24] M. Verbunt, J. Gurtz, K. Jasper, H. Lang, P. Warmerdam, and M. Zappa, "The hydrological role of snow and glaciers in Alpine river basins and their distributed modeling," *J. Hydrol.*, vol. 282, nos. 1–4, pp. 36–55, Nov. 2003.
[25] G. Jouvet, M. Huss, M. Funk, and H. Blatter, "Modelling the retreat of Grosser Aletschgletscher, Switzerland, in a changing climate," *J. Glaciol.*, vol. 57, no. 206, pp. 1033–1045, 2011.
[26] (2019). *SwissTopo*. Accessed: Jan. 19, 2022. [Online]. Available: https://www.swisstopo.admin.ch/fr/geodata/height/alti3d.html
[27] *SwissALTI3D: Le Modèle de Terrain à Haute Résolution de la Suisse*, Office Fédéral de Topographie Swisstopo, Wabern, Switzerland, 2018
[28] R. Hugonnet et al., "Accelerated global glacier mass loss in the early twenty-first century," *Nature*, vol. 592, no. 7856, pp. 726–731, 2021.
[29] S. Leinss and I. Hajnsek, "Seven years of TanDEM-X: Volume loss of Grosser Aletschgletscher, Switzerland," in *Proc. IEEE Int. Geosci. Remote Sens. Symp.*, Jul. 2018, pp. 372–375.

Open Access funding provided by 'Consiglio Nazionale delle Ricerche-CARI-CARE' within the CRUI CARE Agreement